Supporting Information

Unraveling Li-Ion Transport Mechanisms in High-Entropy Anion-Disordered Argyrodites via Machine-Learned Interatomic Potentials

Myeongcho Jang,[a,b,†] Kanguk Park,[a,†] Hun-Gi Jung,[a,c,d] Kyung Yoon Chung,[a,c] Joon Hyung Shim,[b,*] Ohmin Kwon,[a,e,*] Seungho Yu[a,c,*]

[a]Energy Storage Research Center, Korea Institute of Science and Technology, 5, Hwarang-ro 14-gil, Seongbuk-gu, Seoul 02792, Republic of Korea

[b]School of Mechanical Engineering, Korea University, 145 Anam-ro, Seongbuk-gu, Seoul 02841, South Korea

[c]Division of Energy & Environment Technology, KIST School, Korea University of Science and Technology, Seoul 02792, Republic of Korea

[d]Department of Energy Science and KIST-SKKU Carbon-Neutral Research Center, Sungkyunkwan University, Suwon 16419, Republic of Korea

[e]LiB Materials Research Group, Research Institute of Industrial Technology and Science (RIST), POSCO global R&D center, Songdogwahak-ro 100, Yeonsu-gu, Incheon, 21985, Republic of Korea

[†]M. J. and K. P. contributed equally to this work.

[*]Corresponding Authors

Joon Hyung Shim, E-mail: shimm@korea.ac.kr

Ohmin Kwon, E-mail: omkwon0823@posco-inc.com

Seungho Yu, E-mail: shyu@kist.re.kr

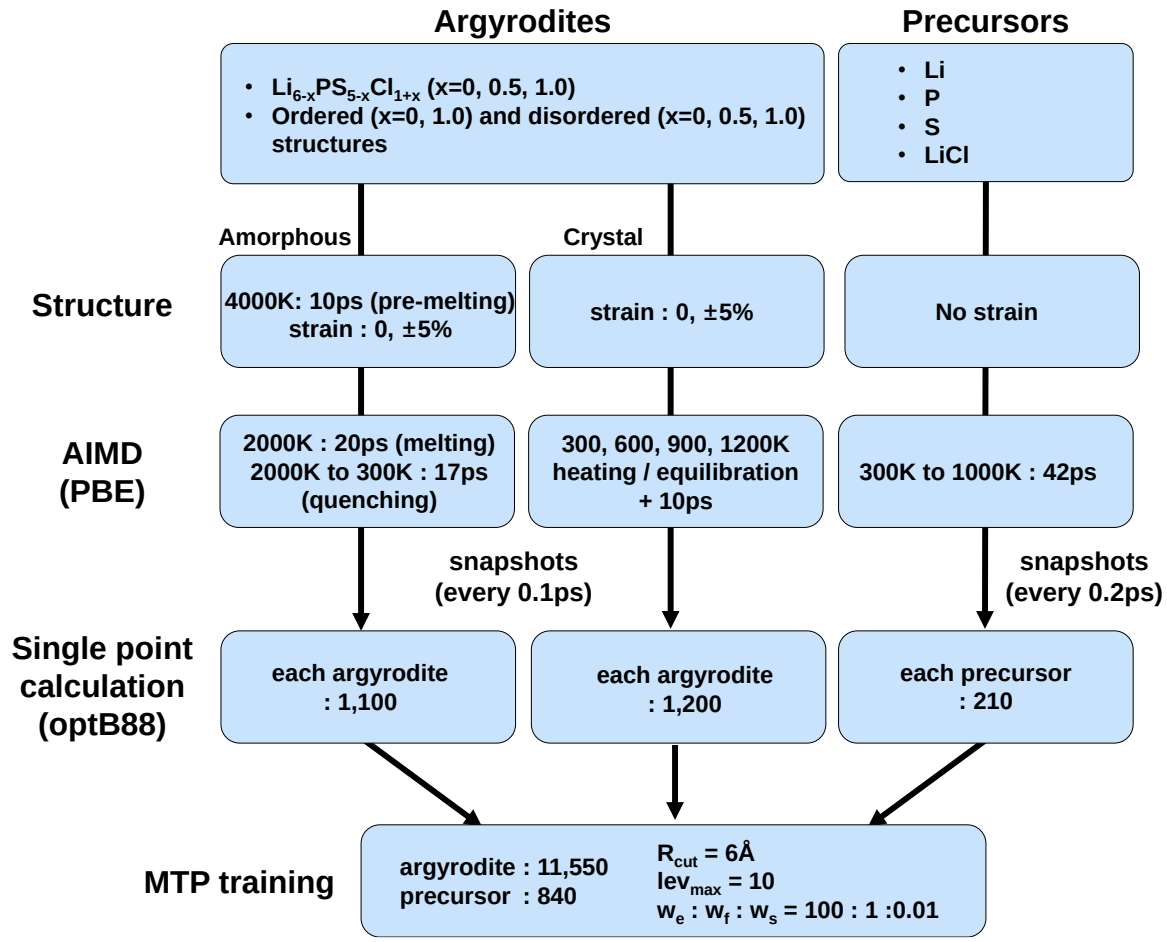

Figure S1. Flowchart of the methods used to develop machine-learned interatomic potentials.

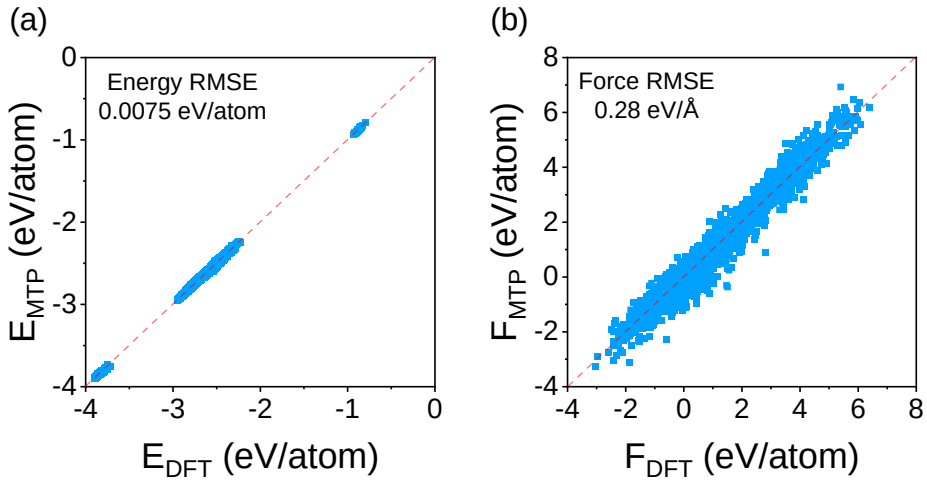

Figure S2. (a) Energy and (b) force calculated using MLIP and DFT for the Li–P–S–Cl system, including RMSE values.

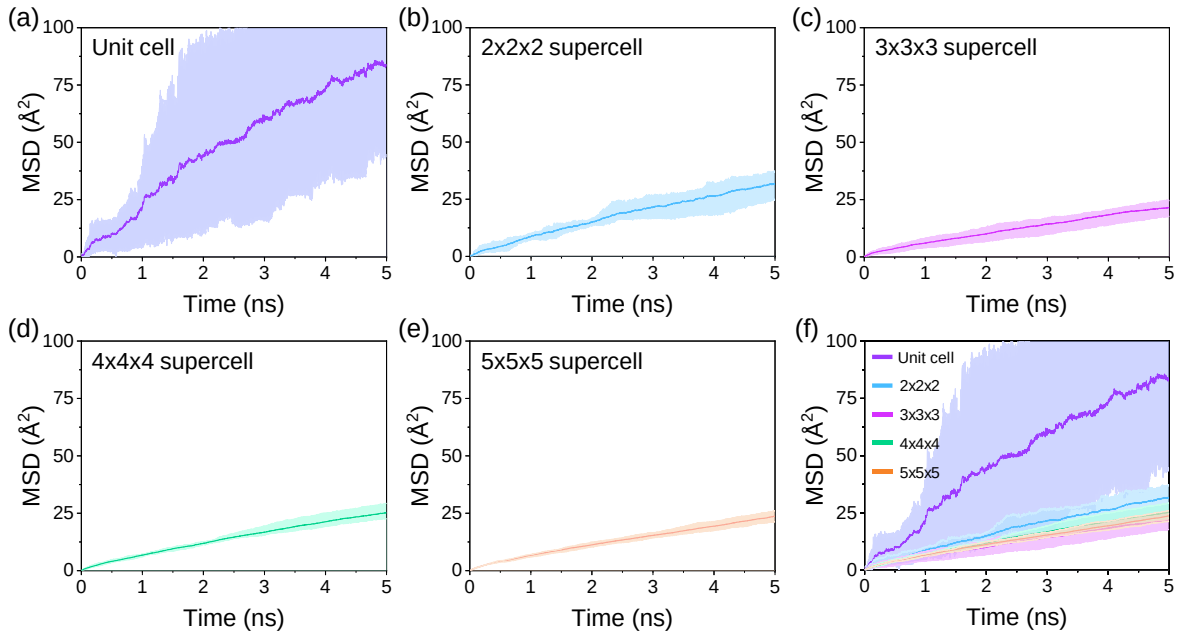

Figure S3. Li-ion MSD values for Li_6PS_5Cl at 300 K using (a) a unit cell, (b) a 2×2×2 supercell, (c) a 3×3×3 supercell, (d) a 4×4×4 supercell, (e) a 5×5×5 supercell, and (f) a comparison plot for (a–e). The MSD values were averaged over five independent MD simulations, and the error range in plots (a-e) represents the maximum and minimum values observed during these five MD simulations.

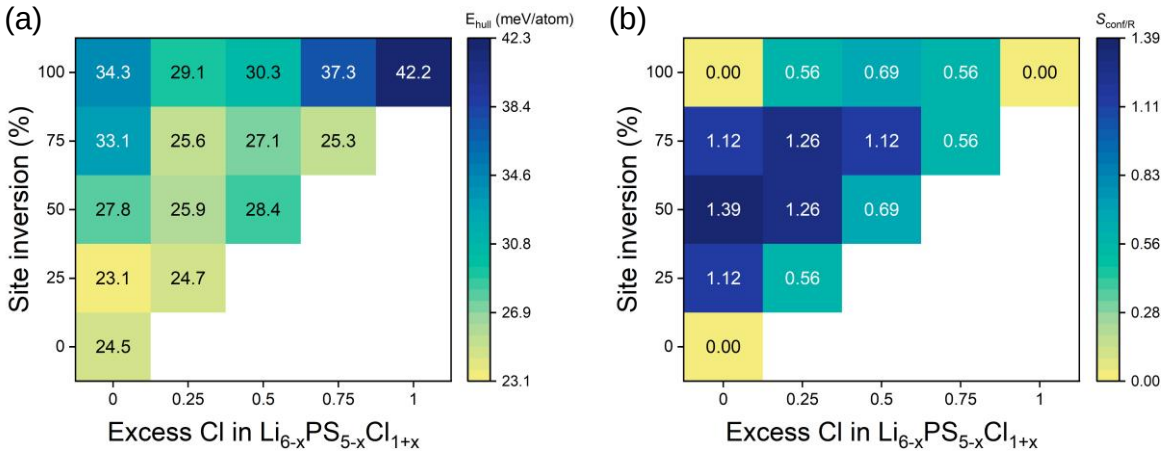

Figure S4. (a) Energy above the hull for $Li_{6-x}PS_{5-x}Cl_{1+x}$ phases with varying degrees of S/Cl site inversion, and (b) their corresponding configurational entropies.

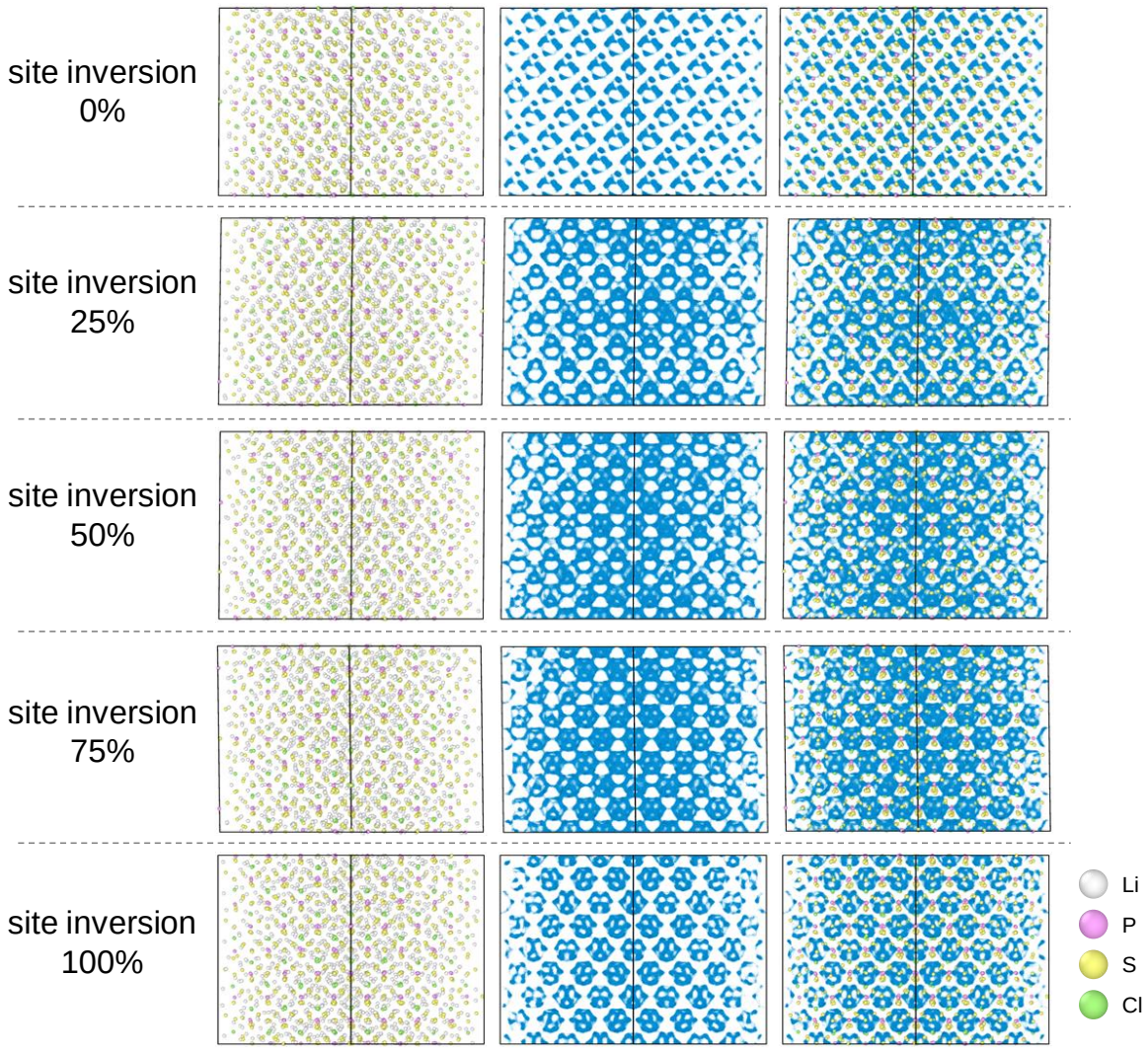

Figure S5. Isosurfaces of the Li-ion probability densities (light blue) for Li_6PS_5Cl with site disorder between the 4a and 4d sites, shown at different degrees of S/Cl site inversion of 0%, 25%, 50%, 75%, and 100%. The left column shows the atomic structures, including Li (white), P (pink), S (yellow), and Cl (green) atoms; the center displays Li-ion trajectories; and the right presents both Li-ion trajectories and atomic structures.

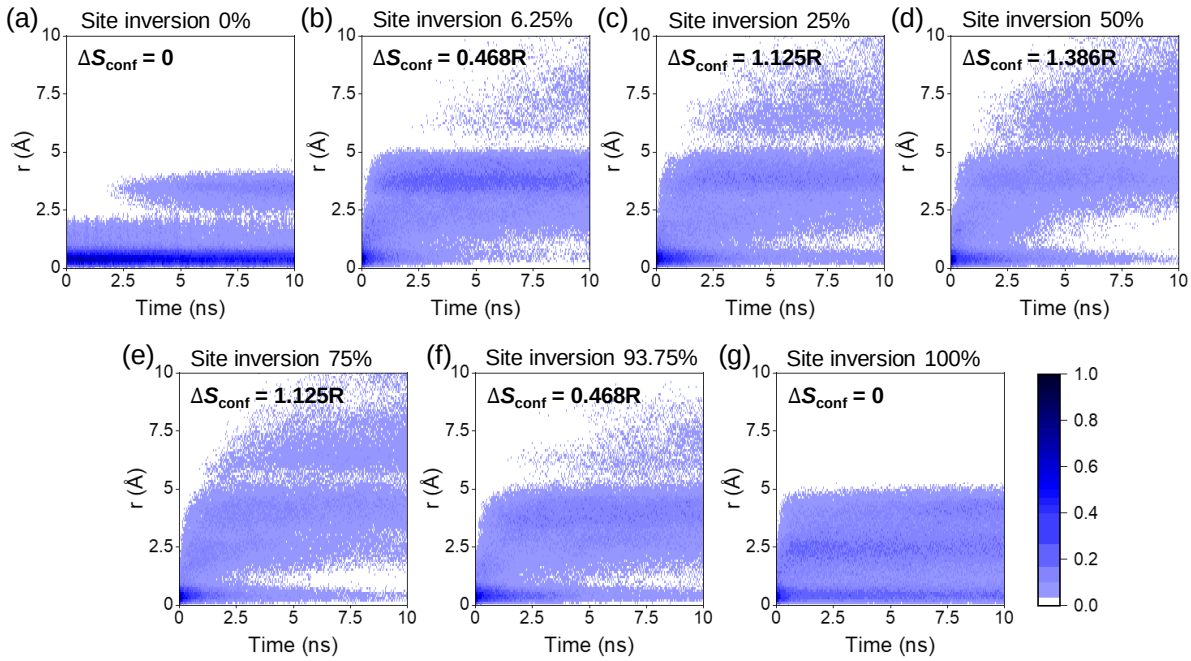

Figure S6. The self-part of the van Hove correlation function in Li_6PS_5Cl as a function of the degree of S/Cl site inversion, ranging from 0% to 100%, based on a 10 ns MD simulation at 300 K, shown for: (a) 0%, (b) 6.25%, (c) 25%, (d) 50%, (e) 75%, (f) 93.75%, and (g) 100%

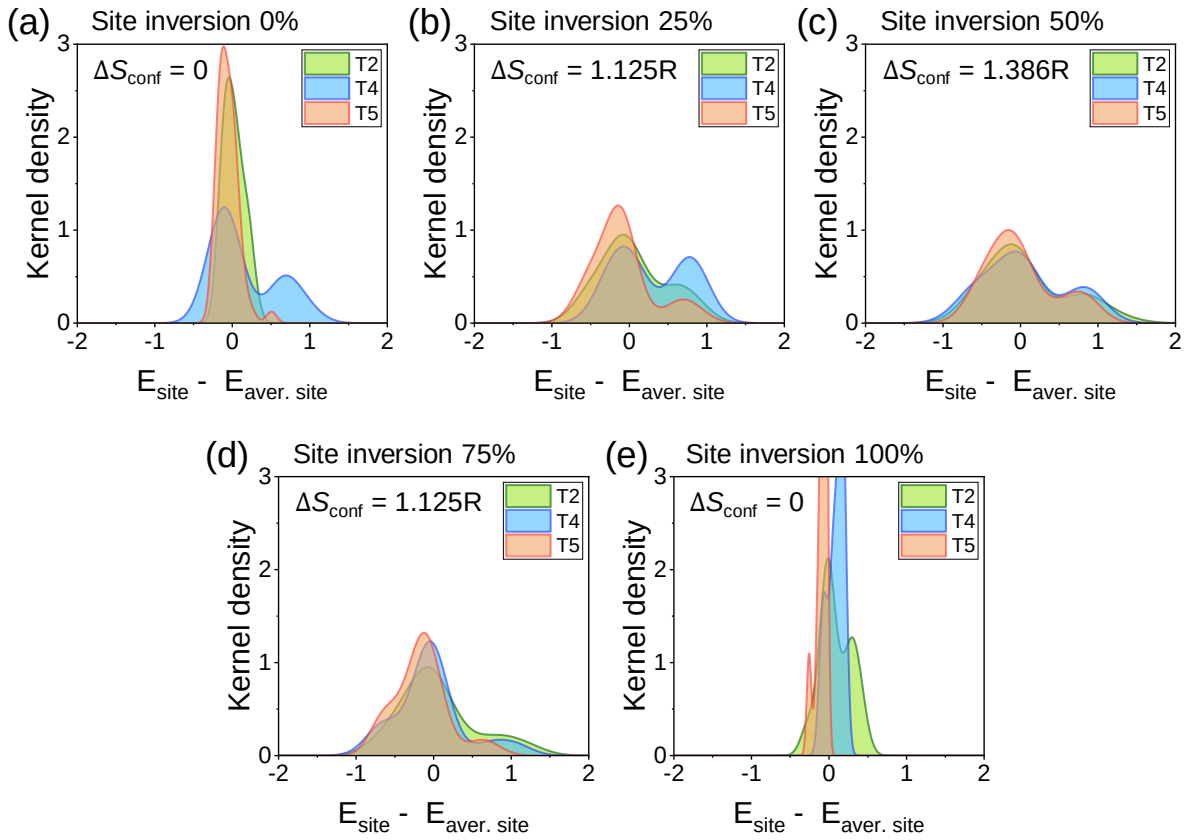

Figure S7. Site energy distributions for Li at the T2, T4, and T5 sites at different degrees of S/Cl site inversion of (a) 0%, (b) 25%, (c) 50%, (d) 75% and (e) 100%.

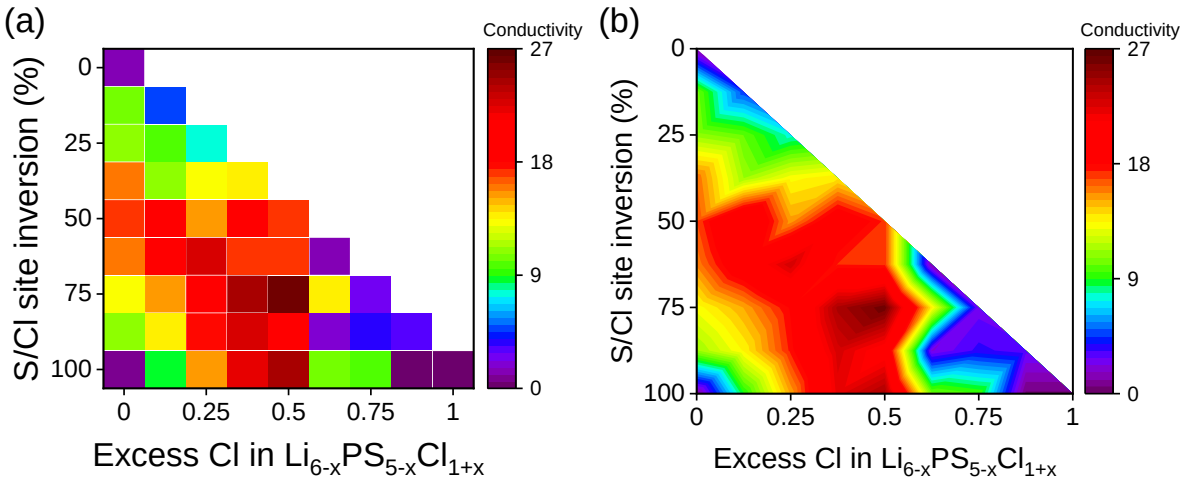

Figure S8. Ionic conductivity of Cl-rich argyrodites $Li_{6-x}PS_{5-x}Cl_{1+x}$ ($0 \leq x \leq 1$) as a function of chlorine content, with varying degrees of S/Cl site inversion: (a) heat map and (b) contour map.

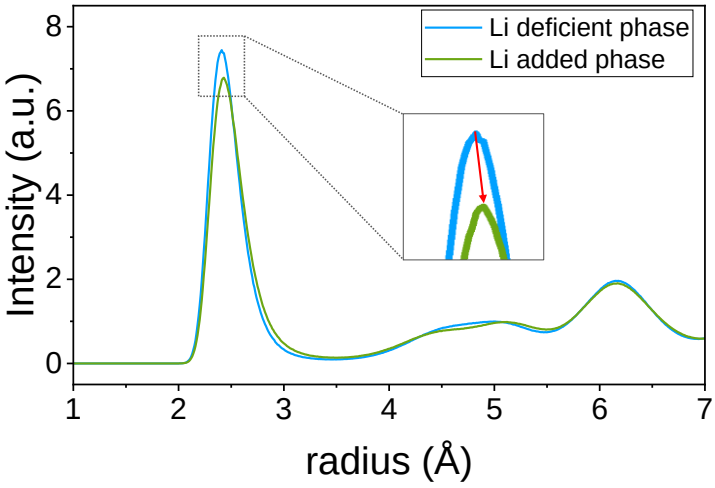

Figure S9. The radial distribution function (RDF) plot for the bonds between all Li and Cl in the 4d sites for the Li-deficient phase, $Li_{5.375}PS_{4.375}Cl_{1.625}$, and the Li-added phase, $Li_6PS_{4.375}Cl_{1.625}$.